Modeling the Local Atomic Structure of Bioactive Sol−Gel-Derived Calcium Silicates

R. N. Mead and G. Mountjoy*

School of Physical Sciences, University of Kent, Canterbury CT2 7NH, United Kingdom

Received December 19, 2005. Revised Manuscript Received June 26, 2006

The current study presents the first detailed models of the local atomic structure in bioactive sol−gel-derived calcium silicates, with the composition $Ca_xSi_{1-x}O_{2-x-y}(OH)_{2y}$, with $0 \leq x \leq 0.5$ and $y = 0.2$, obtained using molecular dynamics. The models are in satisfactory agreement with recent experimental results and show a tetrahedral silica network with network connectivity reduced because of Ca and hydroxyl groups. Ca coordination is ∼6 for a Ca mole fraction of $x = 0.5$ and decreases as $x \rightarrow 0.1$; Ca is coordinated mostly to nonbridging oxygens, but with a small contribution from bridging oxygens. Hydroxyl groups bonded to Si form Si−O−H configurations, but there is also coordination of isolated hydroxyl groups to Ca (which reduces the amount of nonbridging oxygen bonded to Si). There is a substantial contribution to Ca coordination from hydroxyl groups. The Ca distribution for $x = 0.5$ is similar to that seen in $CaSiO_3$ melt-quenched glass models and in neutron diffraction results. For $x \rightarrow 0.1$, there is some clustering of Ca greater than expected for a random distribution. The role of hydroxyl groups in coordinating to Ca is expected to enhance the dissolution of Ca and hence bioactivity.

1. Introduction

The development of new materials for use in tissue replacement therapies is an important area of research and includes bioactive materials that stimulate body cells to generate new tissue.[1] Bioactive materials have been developed for bone replacement therapies.[2,3] These include silica-based melt-quenched glasses (notable among which is "bioglass," with approximate composition $25Na_2O{\cdot}25CaO{\cdot}45SiO_2{\cdot}5P_2O_5$), binary calcium silicate melt-quenched glasses,[4] and recently, binary sol−gel-derived calcium silicates.[5,6] In all of these materials, exposure to simulated body fluid (a protein-free acellular solution with ion concentrations similar to those found in human blood serum[3]) leads to the formation of a calcium phosphate layer as a precursor to bone growth.[7] A key role is played by the silica network, which is acidic and lowers the local pH,[4] and by Ca ions, which are initially rapidly leached and then redeposited in the form of calcium phosphate.[7] Information about the local atomic environments of Si and Ca in these materials is needed to ultimately explain the structural mechanisms for bioactivity.

Bioactive sol−gel-derived calcium silicates are synthesized using a carefully established sol−gel procedure.[6] Along with aging and drying, this procedure includes heat treatment at 600 °C, after which the materials can be considered as being amorphous oxides that are under-dense and hydrated in comparison to melt-quenched glasses. Bioactivity depends on several factors, including porosity and Ca content. Comparison of sol−gel-derived samples with similar porosity has shown that bioactivity is enhanced for a Ca:Si ratio of 3:7.[5,6] Detailed structural studies have recently been carried out, including X-ray and neutron diffraction,[8,9] and Ca K-edge EXAFS.[7] In particular, the advanced method of neutron diffraction with isotopic substitution has been used to observe the Ca environment.[9] The experimental results confirm that the atomic structure is based on a network of SiO_4 tetrahedra, with network connectivity reduced by Ca ions and Ca−O coordinations of 5 to 6. Computer modeling of the local atomic structure will be a very useful complement to experimental work.

The current study presents the first detailed models of the local atomic structure of sol−gel-derived calcium silicates with the composition $Ca_xSi_{1-x}O_{2-x-y}(OH)_{2y}$, which have been obtained using molecular dynamics. The models are compared with experimental results and inspected to identify structural features, including details of the Si and Ca environments. There have been two previously reported modeling studies of $CaSiO_3$ melt-quenched glass,[10,11] and one of sol−gel-derived calcium silicates[12] (the latter presented

* To whom correspondence should be addressed. E-mail: G.Mountjoy@kent.ac.uk. Fax: 44 2337-825-558. Phone: 44 1227-764-000.

(1) Perry C. C. *Chemistry of Advanced Materials*; Interrante, L. V., Hampden-Smith, M. J. Eds.; Wiley: New York, 1998; Chapter 11.
(2) Hench, L. L. *Biomaterials* **1998**, *19*, 1419.
(3) Kokubo, T.; Kim, H. M.; Kawashita, M. *Biomaterials* **2003**, *24*, 2161.
(4) Ylanen, J.; Karlsson, K. H.; Itala, A.; Aro, H. T. *J. Non-Cryst. Solids* **2000**, *275*, 107.
(5) Martinez, A.; Izquierdo-Barba, I.; Vallet-Regi, M. *Chem. Mater.* **2000,** *12*, 3080.
(6) Saravanapavan, P.; Hench, L. L. *J. Non-Cryst. Solids* **2003,** *318*, 1.
(7) Skipper, L. J.; Sowrey, F. E.; Pickup, D. M.; Fitzgerald, V.; Rashid, R.; Drake, K. O.; Lin, Z.; Saravanapavan, P.; Hench, L. L.; Smith, M. E.; Newport, R. J. *J. Biomed. Res.* **2004**, *70A*, 354.
(8) Skipper, L. J.; Sowrey, F. E.; Newport, R. J.; Lin, Z.; Smith, M. E. *Phys. Chem. Glasses* **2005**, *46*, 372.
(9) Skipper, L. J.; Sowrey, F. E.; Pickup, D. M.; Drake, K. O.; Smith, M. E.; Saravanapavan, P.; Hench, L. L.; Newport, R. J. *J. Mater. Chem.* **2005**, *15*, 2369.
(10) Abramo, M. C.; Caccamo, C.; Pizzimenti, G. *J. Chem. Phys.* **1992,** *96*, 9083.
(11) Mead, R. N.; Mountjoy, G. *Phys. Chem. Glasses* **2005**, *46*, 311. Mead R. N.; Mountjoy G. *J. Phys. Chem. B* **2006**, *110*, 14273−14278.
(12) Mead, R. N.; Mountjoy, G. *Mater. Sci. Forum* **2006**, *514−516*, 1059.

10.1021/cm0527975 CCC: $33.50
Published on Web 07/27/2006

limited preliminary results from the current study). In fact, computer modeling is less common for sol−gel-derived materials as compared to melt-quenched glasses. It is worthwhile to develop the use of modeling for such materials, because a number of amorphous oxides are now produced by the sol−gel method. In addition, the current models of sol−gel-derived calcium silicates, when placed in comparison to recent modeling of calcium silicate melt-quenched glasses,[11] provide an insight to underlying differences in local atomic structure between melt-quenched glasses and sol−gel-derived materials.

2. Modeling Method

The molecular dynamics (MD) method for modeling melt-quenched glasses is well-established.[13] A compound is simulated at a series of temperatures decreasing from liquid to solid, with sufficiently rapid quenching of the melt to prevent crystallization. Although the simulated quench rates are always unrealistically high (typically 1×10^{13} K s^{-1}), this method is theoretically equivalent to the melt-quenching process used to form a melt-quenched glass (with quench rates typically 1×10^{3} K s^{-1}). In contrast, the sol−gel process involves gelation,[14,15] takes place on time scales of hours to days, and can be simulated only in a symbolic manner. Previous computer modeling studies of sol−gel-derived materials have focused on mechanisms of the sol−gel process, including aggregation[16,17] and chemical homogeneity,[18] or have assumed such materials to be the same as melt-quenched glasses.[19]

The MD method used in the present study is based on that used for melt-quenched glasses, which meets the key requirement of producing a stable amorphous atomic structure. However, the method is modified to include the two most important differences compared to a melt-quenched glass: sol−gel-derived materials are under-dense and hydrated. Hence, the models have composition $(CaO)_x(SiO_2)_{1-x}(H_2O)_y$ and a lower density than that of corresponding melt-quenched glasses. All H is assumed to be present in hydroxyl groups, because heat treatment at 600 °C will have driven off water molecules (as shown by DTA/TGA results in ref 6), which simplifies the modeling. Thus, the compositions modeled are $Ca_xSi_{1-x}O_{2-x-y}(OH)_{2y}$. The MD quench procedure is still used, not as simulation of the sol−gel process, but as a "simulated annealing" method to find a minimum energy structure. Energy minimization is one of several global optimization procedures that can be employed in a first attempt to find low-energy configurations for systems whose synthesis route itself cannot be modeled. Of course, using such a method ignores the particulars of the synthesis route and risks obtaining models for amorphous structures that lack essential features of the actual compounds.[20]

Table 1. Interatomic Potential Parameters for $Ca_xSi_{1-x}O_{2-x-y}(O_hH)_{2y}$ Models[21]

i	q_i (e)	D_i (eV)	R_i (Å)
Ca	2.1	2.183×10^{-7}	6.243
Si	1.05	7.987×10^{-8}	3.706
O	−1.05	6.744×10^{-3}	3.553
O_h	−0.95	6.744×10^{-3}	3.553
H	0.425		

An interatomic potential for $Ca_xSi_{1-x}O_{2-x-y}(OH)_{2y}$ compounds was obtained from the literature.[21] This potential was previously developed to model clay compounds, and hydroxyl oxygen atoms, denoted O_h, are distinguished from oxide oxygens. This potential described short-range interactions among Ca, Si, and O/O_h using the following two-body term

$$V_{ij}(r) = D_{ij}\left(\left(\frac{R_{ij}}{r}\right)^{12} - 2\left(\frac{R_{ij}}{r}\right)^{6}\right) + \frac{q_i q_j}{4\pi\epsilon_0 r} \qquad (1)$$

where $V_{ij}(r)$ is the potential between elements i and j as a function of distance r, q are charges, and $D_{ij} = (D_iD_j)^{1/2}$ and $R_{ij} = (R_i + R_j)/2$ are potential parameters. The potential parameters are shown in Table 1. For the hydroxyl group, i.e., O_hH, the following two-body term was used

$$V_{O_hH}(r) = k_1(r_{O_hH} - r_0)^2 \qquad (2)$$

where $k_1 = 24.05$ eV Å^{-2} and $r_0 = 1.00$ Å are the potential parameters. (The original potential included a three-body term for Ca/Si−O_h−H bond-bending interactions, but this was only considered important for modeling interfacial structures[21] and was not included in the current study.)

The potential was evaluated by using the GULP program[22] to model crystalline $Ca_xSi_{1-x}O_{2-x-y}(OH)_{2y}$ compounds: lime CaO,[23] quartz SiO_2,[24] wollastonite $CaSiO_3$,[25] portlandite $Ca(OH)_2$,[26] alpha dicalcium silicate $Ca_2(SiO_3OH)(OH)$,[27] dellaite $Ca_6(Si_2O_7)(SiO_4)(OH)_2$,[28] and rosenhahnite $Ca_3(Si_3O_8(OH)_2)$[29] (the crystal structure data was obtained from CDS[30]). In addition, the molecular structures of mono- and trisilicilic acid $[Si(OH)_4]_n$ were modeled.[31] The results are quite accurate, considering that nine structures are described by a potential with only 15 parameters. The results are slightly less accurate than those from an interatomic potential dedicated to only $(CaO)_x(SiO_2)_{1-x}$ compounds,[11] giving Si−O distances that are too short by ∼0.03 Å and Ca−O distances that are too long by ∼0.03 Å. (Previous studies have noted

(13) Du, J.; Cormack, A. N. *J. Non-Cryst. Solids* **2001,** *293*−*295*, 283.
(14) Flory, P. J. *Principles of Polymer Chemistry*; Cornell University Press: Ithaca, NY, 1953.
(15) Stauffer, D. *Physica A* **1981**, *106*, 177.
(16) Kolb, M.; Herrmann, H. J. *J. Phys. A* **1985**, *18*, L435.
(17) Jullien, R.; Hasmy, A. *Phys. Rev. Lett.* **1995**, *74*, 4003.
(18) Hannemann, A.; Schon, J. C.; Jansen, M. *J. Mater. Chem.* **2005**, *15*, 1167.
(19) Petkov, V.; Holzhuter, G.; Troge, U.; Gerber, T.; Himmel, B. *J. Non-Cryst. Solids* **1998**, *231*, 17.
(20) Hannemann, A.; Schon, J. C.; Jansen, M.; Putz, H.; Lengauer, T. *Phys. Rev. B* **2004**, *70*, 144201.
(21) Cygan, R. T.; Liang, J. J.; Kalinichev, A. G. *J. Phys. Chem. B* **2004**, *108*, 1255.
(22) Gale, J. D. *J. Chem. Soc., Faraday Trans.* **1997**, *93*, 629.
(23) Natta, G.; Passerini, L. *Gazz. Chim. Ital.* **1929**, *59*, 129.
(24) Norby, P. *J. Appl. Cryst.* **1997**, *30*, 21.
(25) Ohashi, Y. *Phys. Chem. Mineral.* **1984,** *10*, 217.
(26) Desgranges, L.; Grebille, D.; Calvarin, G.; Chevrier, G.; Floquet, N.; Niepce, J.-C. *Acta Crystallogr., Sect. B* **1995**, *49*, 812.
(27) Marsh, R. E. *Acta Crystallogr., Sect. C* **1994**, *50*, 996.
(28) Safronov, A. N.; Nevskii, N. N.; Ilyukhin, V. V.; Belov, N. V. *Dokl. Akad. Nauk SSSR* **1981**, *256*, 1387.
(29) Cheng, W.; Ghose, S.; Gibbs, G. V. *Nature* **1977**, *241*, 42.
(30) Fletcher, D. A.; McMeeking, R. F.; Parkin, D. *J. Chem. Inf. Comput. Sci*. **1996**, *36*, 746.
(31) Hill, J. R.; Sauer, J. *J. Phys. Chem.* **1994**, *98*, 1238.

Table 2. Details of $Ca_xSi_{1-x}O_{2-x-y}(O_hH)_{2y}$ Models Obtained in This Study (note: all models have $y = 0.2$, except model $x = 0.3$ DH with $y = 0.3$; also shown are experimental densities of melt-quenched[9] and sol−gel-derived[38] glasses)

x	melt-quenched density (g cm^{-3}) ±0.02	sol−gel-derived density (g cm^{-3}) ±0.10	model density (g cm^{-3})	model atoms	model length (Å)
0.5	2.90	2.45	2.67	992	23.08
0.4	2.78	2.40	2.50	1024	23.62
0.3	2.63	2.50	2.37	1056	24.11
0.3 D			2.23	1056	24.55
0.3 DH			2.23	1044	23.87
0.2	2.47	2.35	2.22	1088	24.67
0.1	2.33		2.10	1120	25.18
0	2.19		1.99	1152	25.72

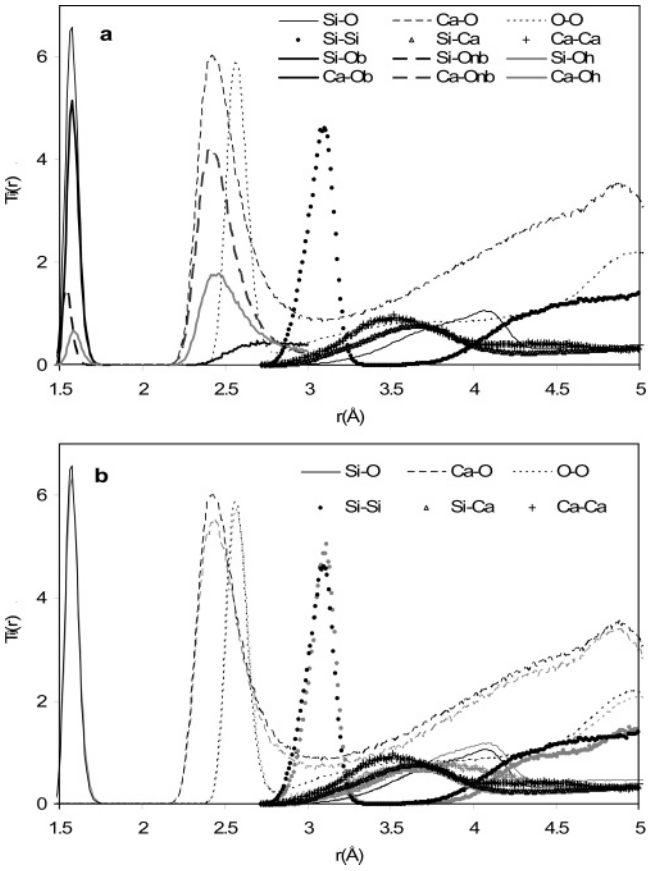

Figure 1. (a) Radial distribution functions, $T_{ij}(r)$, for the $x = 0.3$ model, including distinction between bridging O_b, nonbridging O_{nb}, and hydroxyl O_h, oxygens. (b) (black) Radial distribution functions, $T_{ij}(r)$, for the $x = 0.3$ model and (grey) after an additional NPT simulation at 600 K for 80 000 time steps. (Si−O correlations have been scaled ×1/4 and O−O correlations have been scaled by ×1/2).

that Ca−O distances tend to be overestimated in the modeling of glasses.[32])

Molecular dynamics modeling was used to obtain models of atomic structure of amorphous $Ca_xSi_{1-x}O_{2-x-y}(OH)_{2y}$ with Ca mole fractions of $x = 0$, 0.1, 0.2, 0.3, 0.4, and 0.5 and $y = 0.2$, which includes the range of experimental compositions. Each model has ∼1000 atoms in a cubic box with length ∼25 Å. This size is typical for modeling amorphous materials (balancing computational time and sampling of a large amorphous structure), and is $\sim 5^3\times$ larger than the features of the local atomic structure that are of interest in the current study. Table 2 shows the details of the models. Experimental data[7−9] was used to estimate the hydroxyl content (from inductively coupled plasma analysis) and density (from N_2 gas adsorption, He pycnometry, and TGA). Hydroxyl content was estimated to be $y = 0.2$ (∼12 atm % H), and density was estimated to be 90% of $(CaO)_x(SiO_2)_{1-x}$ melt-quenched glass density,[33] for all x. The values of model density range from 1.99 g cm^{-3} for $x = 0$ to 2.67 g cm^{-3} for $x = 0.5$. (Note that density refers to the skeletal density and excludes pore volumes but allows for additional volume associated with skeletal Si−O−H groups.) In addition, models with $x = 0.3$ were made with a density of 85% (model denoted $x = 0.3$ D) and hydroxyl content of $y = 0.3$ (model denoted $x = 0.3$ DH), to check the sensitivity of local atomic environments in model structures to these parameters.

The molecular dynamics modeling used the DLPOLY program,[34] with time steps of 0.5 fs, a short-range cutoff of 10 Å, and Coulomb potential calculated using the Ewald sum method. A Berensden NVT algorithm was used (with relaxation time of 2 ps) to achieve the objective of models matching the experimental density. Random starting configurations and periodic boundary conditions were used. The modeling incorporated three stages of 160 000 time steps with temperature baths at 6000, 4000, and 2000 K, with linear thermal expansion coefficients of 1.03, 1.015, and 1.05, respectively, with respect to the target density. This was followed by a temperature quench of 85 000 time steps from 2000 to 300 K (i.e., 5 time steps per K). Finally, there were two stages of 160 000 time steps with the temperature bath at 300 K. Structural parameters were sampled during the last stage (every 200 time steps) to include the effects of disorder due to thermal vibrations.

The models obtained in the current study have a local atomic structure that can be viewed as being realistic to the extent that it has minimum energy with respect to interatomic potentials and as being representative to the extent that it agrees with experimental results (see Section 3.4). The reproducibility was checked by building a second model of the $x = 0.3$ composition, and the structural parameters obtained were the same within statistical noise. The stability was checked by putting the $x = 0.3$ model into additional simulations, each of 80 000 time steps. An NVT simulation at 600 K resulted in no changes in structure apart from thermal vibrations. At 900 K, there was no change in the silica network structure, but some diffusion of Ca and segregated hydroxyl groups (i.e., those not bonded to Si). An NPT simulation at 1 atm and 600 K resulted in an (initial) 4% decrease in density with no change in connectivity of

(32) Delaye, J. M.; Cormier, L.; Ghaleb, D. L.; Calas, G. *J. Non-Cryst. Solids* **2001,** *293−295*, 290.
(33) Doweidar, H. *J. Non-Cryst. Solids* **1999**, *249*, 194.
(34) Smith, W.; Forester, T. *J. Mol. Graphics* **1996**, *14*, 136.

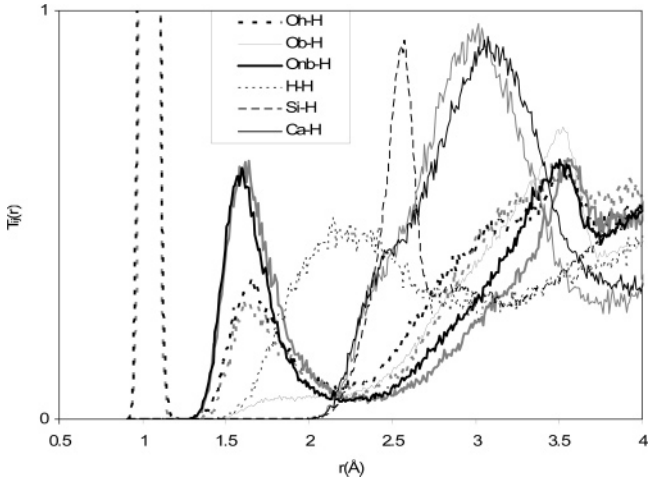

Figure 2. (black) Radial distribution functions involving hydrogen, i.e., $T_{i-H}(r)$, for the $x = 0.3$ model and (grey) after an additional NPT simulation at 600 K for 80 000 time steps (in the latter, O_b−H, Si−H, and H−H correlations have been omitted for clarity).

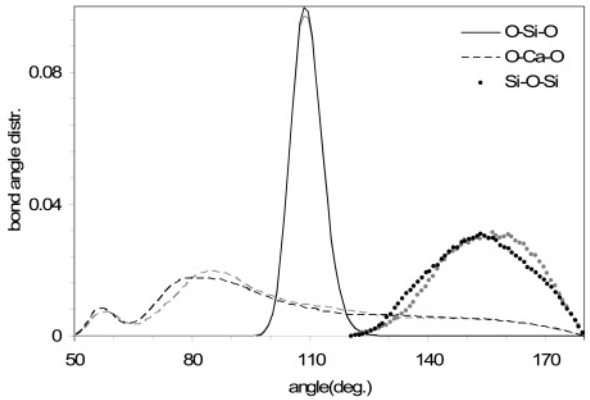

Figure 3. (black) Bond angle distributions for the $x = 0.3$ model and (grey) after an additional NPT simulation at 600 K for 80 000 time steps. (Note that O refers to all types of oxygen.)

atoms in the silica network, but some changes in positions of Ca. It resulted in only slight changes to $T_{ij}(r)$ and bond angle distributions, as shown in Figures 1b, 2, and 3 . (Note that the current study used an NVT algorithm to achieve the objective of matching the experimental density.)

3. Results

3.1. Short-Range Order. The results are first shown in detail for the $x = 0.3$ model, before considering variations in structure due to the Ca mole fraction (x), density, and hydroxyl content (y). Figure 1 shows the radial distribution functions $T_{ij}(r)$ for the $x = 0.3$ model (excluding correlations involving H), where

$$T_{ij}(r) = \frac{1}{r}\left(\frac{1}{N_i}\sum_{i=1}^{N_i}\sum_{j\neq i}^{N_j}\delta(r - R_{ij})\right) \qquad (3)$$

and $T_{ij}(r) \rightarrow 4\pi r\rho_{0j}$ as $r \rightarrow \infty$. The first peak in $T_{SiO}(r)$ at ∼1.6 Å represents distances between Si−O nearest neighbors. In all of the models, >99% Si has exactly 4-fold coordination, and the O−Si−O bond angle is tetrahedral, as shown in Figure 3. The first peak in $T_{CaO}(r)$ at ∼2.4 Å

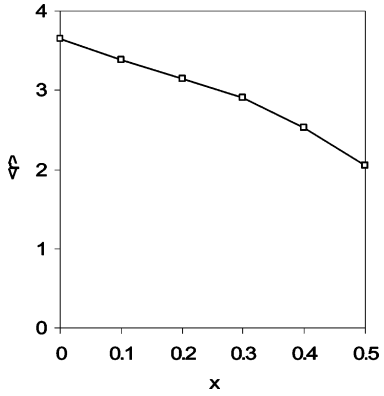

Figure 4. Average connectivity of the silica network ⟨r⟩, from $x = 0$ to $x = 0.5$.

represents distances between Ca−O nearest neighbors (discussed below). $T_{OO}(r)$ has a first peak at ∼2.6 Å that represents O coordinated to Si, i.e., O−Si−O configurations; this is followed by a broad peak at 3.0−3.5 Å that represents O coordinated to Ca, i.e., O−Ca−O configurations. $T_{SiSi}(r)$ has a first peak at ∼3.1 Å that represents Si−Si nearest neighbors in the silica network, which have an average Si−O−Si bond angle of ∼150° (Figure 3). Si−Ca and Ca−Ca correlations overlap and are first prominent in the region 3.1−3.6 Å.

Figure 2 shows correlations involving H, i.e., $T_{i-H}(r)$. The first peak in $T_{O_hH}(r)$ at 1.05 Å represents hydroxyl groups, which have a well-defined interatomic distance due to the potential in eq 2. The second peak in $T_{O_hH}(r)$ at ∼1.8 Å represents hydroxyl oxygen, which is near to hydrogen in a different hydroxyl group and hence represents hydrogen bonding. There is similar a peak in $T_{OH}(r)$, where O denotes non-hydroxyl oxygens (i.e., not directly bonded to H). The first peak in $T_{HH}(r)$ at ∼2.1 Å can also be attributed to hydrogen bonding between hydroxyl groups. The first peak in $T_{SiH}(r)$ at ∼2.6 Å is a consequence of Si coordinated to O_h (which in turn is coordinated to H). Similarly, the first peak in $T_{CaH}(r)$ at ∼3.0 Å occurs because of Ca being coordinated to O_h.

3.2. Silica Network Connectivity. The silica network connectivity is described in terms of linkages between SiO_4 tetrahedra. Non-hydroxyl oxygens linking 2 Si nearest neighbors are classified as bridging oxygens, denoted O_b, otherwise as nonbridging oxygens, denoted O_{nb}. Hydroxyl oxygens are separately classified (denoted O_h), and hydroxyls can behave like Si−O_{nb} configurations because both contain a singly bonded oxygen. The average connectivity of Si is $\langle r\rangle = N_{SiO_b}$, i.e., the number of bridging oxygens per Si, and a fully connected SiO_2 network has $\langle r\rangle = 4$. The values of $\langle r\rangle$ are shown in Figure 4. As expected for $x = 0$, the silica network connectivity is already reduced, because of the presence of hydroxyls. The value of $\langle r\rangle$ can be accurately predicted from $SiO_{2-y}(OH)_{2y} \rightarrow SiO_{4-\langle r\rangle/2}H_{2y}$, which for $y = 0.2$ gives $\langle r\rangle = 3.6$, consistent with $N_{SiOb} = 3.54$ shown in Table 3.

Increasing the Ca content causes a further reduction in the connectivity of the silica network, as expected, with decreasing average ⟨r⟩ as shown in Figure 4. Interestingly, for $x \rightarrow 0.5$, the connectivity is greater than expected if both

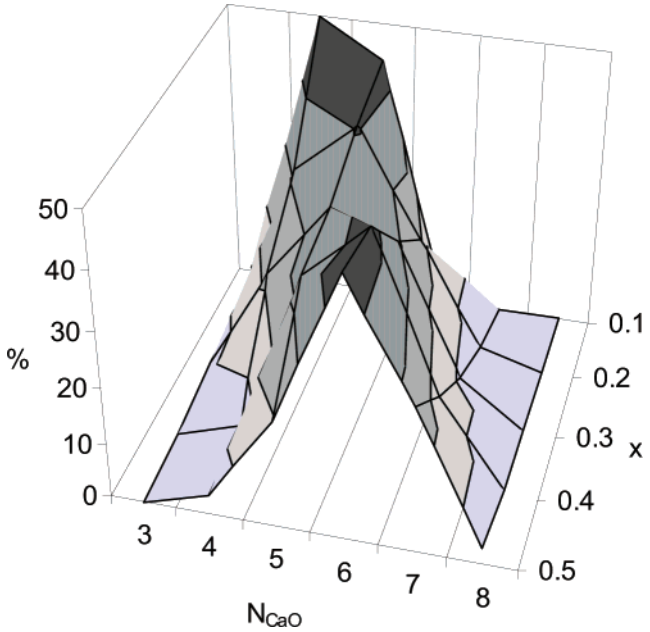

Figure 5. Distribution of Ca−O coordination numbers, i.e., N_{CaO}, from $x = 0$ to $x = 0.5$. (Note that O refers to all types of oxygen.)

Table 3. Average Nearest-Neighbor Distances *R* and Coordination Numbers *N* for Interatomic Correlations Involving Si

x	R_{SiO} (Å)	N_{SiO}	N_{SiOnb}	$N_{SiOb} = N_{SiSi}$	N_{SiOh}
0	1.58	3.99	0.03	3.54	0.40
0.1	1.58	4.00	0.20	3.38	0.40
0.2	1.58	4.00	0.43	3.15	0.41
0.3	1.57	4.00	0.69	2.90	0.43
0.3D	1.57	4.00	0.72	2.84	0.44
0.3DH	1.57	4.00	0.62	2.61	0.77
0.4	1.57	4.00	1.07	2.53	0.42
0.5	1.57	4.00	1.55	2.05	0.42

hydroxyls and Ca break Si−O−Si connections. Assuming all O (including O_h) is coordinated to Si gives $Ca_xSi_{1-x}O_{2-x-y}(OH)_{2y} \rightarrow Ca_{x/(1-x)}SiO_{4-\langle r\rangle/2}H_{2y/(1-x)}$ or

$$4 - \frac{\langle r\rangle}{2} = \frac{2 + y - x}{1 - x} \quad (4)$$

Solving this for $y = 0.2$ gives $\langle r\rangle = (3.6 - 6x)/(1 - x)$, which for $x = 0.5$ gives $\langle r\rangle = 1.2$. In contrast, Table 3 shows $N_{SiOb} = 2.05$ for $x = 0.5$, so the network connectivity observed is greater than the predicted $\langle r\rangle = 1.2$. This implies that some of the oxygen has no bond to Si (see Discussion).

3.3. Ca Coordination. The Ca−O coordination, i.e., N_{CaO}, was defined using the minimum in $T_{CaO}(r)$ at ∼3.0 Å. The distribution of N_{CaO} is shown in Figure 5, and the average of N_{CaO} decreases from 6.0 for $x = 0.5$ to 4.5 for $x = 0.1$, as shown in Table 4. The O−Ca−O bond angle distribution shown in Figure 3 for $x = 0.3$ represents CaO_N polyhedra and peaks at ∼80°, extending to 180° as expected for typically distorted 6-fold coordination. The small peak at ∼60° in the O−Ca−O bond angle distribution is mostly due to O_{nb}−Ca−O_b configurations in which the two oxygens are part of the same SiO_4 tetrahedra (i.e., edge-sharing between SiO_4 and CaO_N polyhedra). Table 4 shows the contribution to Ca−O coordination from different types of oxygen, i.e., $N_{CaO_{nb}}$, N_{CaO_b}, and N_{CaO_h}. As expected, most of the Ca−O coordination is due to O_{nb}, with the average of $N_{CaO_{nb}}$ decreasing from 3.7 for $x = 0.5$ to 2.4 for $x = 0.1$. However, there is a substantial contribution from O_h, with the average $N_{CaO_h} \approx 1.6$ for all x, and a small contribution from O_b, with the average $N_{CaO_b} \approx 0.6$ for all x.

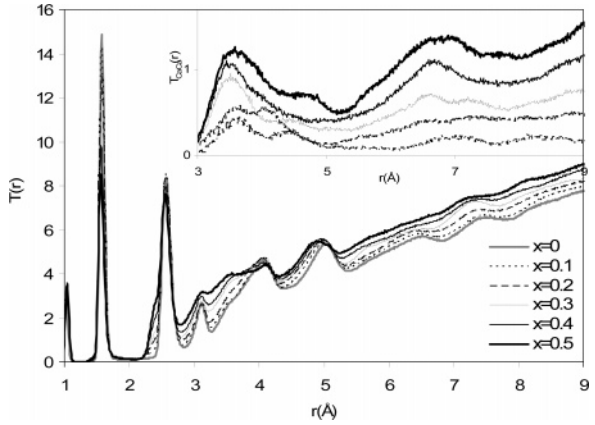

Figure 6. Total radial distribution functions, $T(r)$, from $x = 0$ to $x = 0.5$. The inset shows $T_{CaCa}(r)$.

Table 4. Average Nearest-Neighbor Distances *R* and Coordination Numbers *N* for Interatomic Correlations Involving Ca

x	R_{CaO} (Å)	N_{CaO}	N_{CaOnb}	N_{CaOb}	N_{CaOh}	N_{CaCa}
0						
0.1	2.39	4.49	2.38	0.55	1.57	1.89
0.2	2.42	4.89	2.85	0.55	1.49	2.79
0.3	2.43	5.33	3.12	0.59	1.62	3.97
0.3D	2.43	4.99	3.14	0.37	1.48	3.95
0.3DH	2.43	5.27	2.52	0.38	2.37	3.38
0.4	2.43	5.73	3.42	0.57	1.74	4.94
0.5	2.43	5.97	3.67	0.48	1.83	6.65

3.4. Comparison with Experimental Values. The total $T_{ij}(r)$ (with $T(r) = \Sigma_{ij}T_{ij}(r)$ and $T(r) \rightarrow 4\pi r\rho_0$ as $r \rightarrow \infty$) has a predictable dependence on x. Figure 6 shows that increasing x from 0 to 0.5 causes a decrease in the peaks at ∼1.6 and ∼3.1 Å because of Si−O and Si−Si nearest neighbors, respectively. (The peak at ∼2.6 Å due to O−Si−O configurations does not decrease much because of the combined effects of reduced Si content and reduced network connectivity.) At the same time, there is an increase in the height of features at ∼2.4, 3.0−3.5, and 3.1−3.6 Å that correspond to Ca−O nearest neighbors, O−Ca−O configurations, and Si−Ca/Ca−Ca correlations, respectively. The peak at 1.0 Å due to hydroxyl groups remains constant (because y is constant). The changes occurring in $T_{ij}(r)$ give changes in the diffraction structure factor $S(Q)$, with

$$Q(S(Q) - 1) = \sum_{ij} w_{ij}(Q) \int (T_{ij}(r) - 4\pi r\rho_{0j})\sin(Qr)dr \quad (5)$$

where $w_{ij}(Q)$ is the weighting factor for scattering from correlations between elements i and j. Figure 7 shows the calculated X-ray diffraction $S(Q)$ for models with x from 0.2 to 0.5. ($S(Q)$ values were calculated using $T_{ij}(r)$ up to an r value of 10 Å, for which case a cutoff function was found to be unnecessary.)

The current modeling results can be compared with the previous experimental work on sol−gel-derived calcium silicates. Table 5 shows experimental results for $x = 0.3$ obtained from neutron diffraction with isotopic substitution[9] and Ca K-edge EXAFS.[7] The neutron diffraction data was

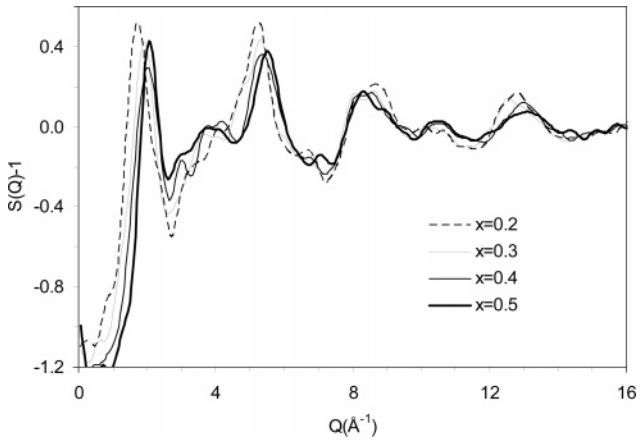

Figure 7. Calculated X-ray diffraction structure factors $S(Q)$ for models, from $x = 0.2$ to $x = 0.5$.

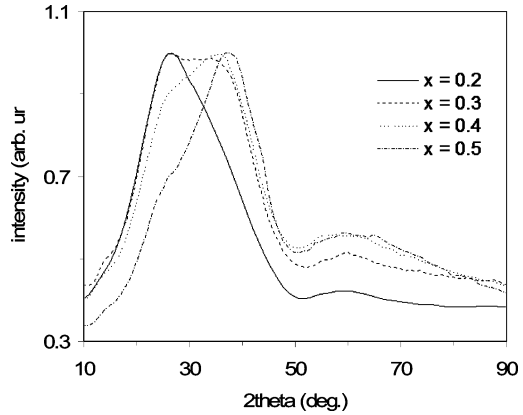

Figure 8. Experimental X-ray diffraction structure factors $S(Q)$,[8] from $x = 0.2$ to $x = 0.5$.

Table 5. Comparison of Modeling and Experimental Results for $x = 0.3$ (Note that O refers to all types of oxygen.)

	MD	neutron diffraction[9]	EXAFS[7]
R_{SiO} (Å)	1.57	1.60(1)	
N_{SiO}	4.0	3.8(3)	
R_{CaO} (Å)	2.43	2.40(1)	2.32(1)
N_{CaO}	5.3	5.0(3)	5.2(3)
R_{OO} (Å)	2.58	2.64(1)	
N_{OO}	4.5	4.6(3)	

fitted using three Ca−O correlations, with $R_{CaO} = 2.32/2.51/2.75$ Å and $\mathbf{N}_{CaO} = 2.30/1.65/1.05$, respectively. Table 5 shows the equivalent values for a single Ca−O correlation, which are $R_{CaO} = 2.40$ Å and $N_{CaO} = 5.0$. The $x = 0.3$ model results of $R_{CaO} = 2.43$ Å and $N_{CaO} = 5.3$ are in good agreement. The EXAFS results are $N_{CaO} = 5.2$, which is also in agreement, and $R_{CaO} = 2.32$, which seems short compared to both neutron diffraction and the $x = 0.3$ model. (Very similar EXAFS results were obtained for $x = 0.2$, 0.3, 0.4, and 0.5,[7] and the same comments apply in comparison to the models.)

The experimental X-ray diffraction results, shown in Figure 8, highlight the shift in the first sharp diffraction peak to larger angles as x increases from 0.2 to 0.5. This was previously interpreted as a "fingerprint" of Ca content.[8] The modeling results shown in Figure 7 show the same behavior, with the first sharp diffraction peak increasing from $Q = 1.7$ Å^{-1} to $Q = 2.1$ Å^{-1} as x increases from 0.2 to 0.5 (where $Q = 4\pi\sin(\theta)/\lambda$, 2θ is the angle, and λ is the wavelength). As discussed, the composition $x = 0.3$ has been the focus

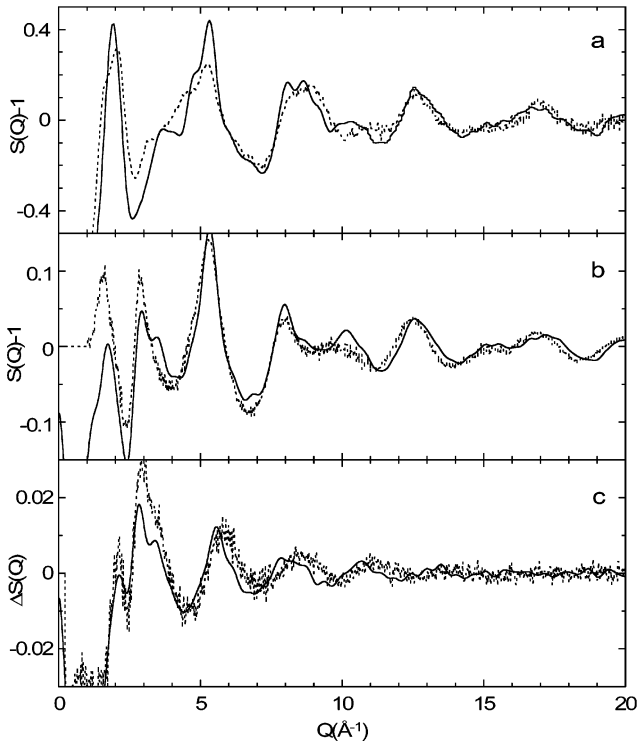

Figure 9. Structure factors $S(Q)$ for $x = 0.3$ from (solid line) the model and (dotted line) the experiment[9] for (a) X-ray diffraction, (b) neutron diffraction, and (c) single difference $\Delta S(Q)$ for neutron diffraction with isotopic substitution.

of recent experimental studies[7,8,9]. Figure 9 shows the structure factors $S(Q)$ obtained from X-ray and neutron diffraction for $x = 0.3$,[9] and the results for the $x = 0.3$ model are in good agreement. (There is a discrepancy at low Q for X-ray diffraction, which may indicate differences in medium-range order or uncertainty in background subtraction of experimental data, because the experimental value of $S(Q) \rightarrow 1$ for low Q is unrealistic.) Furthermore, neutron diffraction with isotopic substitution was used to measure the single-difference structure factor $\Delta S(Q)$,[9] which is also shown in Figure 9. This is an advanced measurement that gives the change in neutron scattering when ^{44}Ca is substituted for ^{nat}Ca, defined by $\Delta S(Q)$, where

$$Q(\Delta S(Q) - 1) = \sum_{Ca-j} \Delta w_{Ca-j}(Q) \int (T_{Ca-j}(r) - 4\pi r \rho_{0j}) \sin(Qr) dr \quad (6)$$

and $\Delta w_{Ca-j}(Q)$ is the change in weighting factor for scattering from correlations between elements Ca and j (see ref 9). Hence, $\Delta S(Q)$ gives information about the local atomic environment of Ca (see Table 5). Again, the $x = 0.3$ model is in fair agreement. It is apparent that the period of oscillations in the model $\Delta S(Q)$ is slightly short compared to the experimental value. This is due to the Ca−O potentials giving an average Ca−O bond length that is slightly too long (as noted in previous modeling studies of glasses[32]).

4. Discussion

4.1. Comparison with Calcium Silicate Melt-Quenched Glass Models. The analysis of the $Ca_xSi_{1-x}O_{2-x-y}(OH)_{2y}$ models provides a detailed picture of the atomic structure,

and in particular the local atomic environments of Si and Ca. Si and Ca display behavior similar to that seen in recent models of $CaSiO_3$ melt-quenched glass.[11] Si forms a tetrahedral silica network, and the main contributions to Si−O coordination are from O_b and O_{nb}. As expected, increasing x corresponds with the silica network connectivity being reduced by Ca, with increasing Si coordination to O_{nb}. Ca acts as a network modifier and prefers a coordination of 6 or higher.[35] Ca is predominantly coordinated to O_{nb}, with a small contribution from O_b ($N_{CaOb} \approx 0.6$) for all Ca mole fractions x. For $x = 0.5$, the average Ca−O coordination is $N_{CaO} = 6.0$, and the CaO_N polyhedra can be described as being distorted octahedra, which are reminiscent of octahedra present in crystalline $CaSiO_3$ wollastonite. For $x \rightarrow 0.1$, the coordination decreases noticeably below 6, because of a decrease in $N_{CaO_{nb}}$. In these respects, the behavior is similar to that seen in models of melt-quenched glasses, but in other respects, there are dramatic differences.

4.2. Effect of Hydroxyls on Silica Network Connectivity. The major difference from melt-quenched glasses is the significant content of hydroxyl groups, which was one of the motivations for the current study. The presence of hydroxyls affects Si by forming a small contribution to Si−O coordination ($N_{SiO_h} \approx 0.4$) and reducing the silica network connectivity. The hydroxyls are responsible for reduced network connectivity at $x = 0$. As discussed in the Results section, assuming all oxygens are coordinated to Si enables the network connectivity to be predicted from the Si to O ratio, according to eq 4. For $x = 0$ and $y = 0.2$, eq 3 gives $\langle r \rangle = 3.6$, which agrees with the observed value $N_{SiO_h} = 0.4$. However, for $x = 0.5$ and $y = 0.2$, eq 4 gives $\langle r \rangle = 1.2$, which is much less than the observed value $N_{SiO_b} = 2.0$.

To explain why the network connectivity is higher than expected for $x \rightarrow 0.5$, it is informative to consider the separate contributions to eq 4 from Ca and hydroxyls. For Ca, the contribution to eq 4 is $x/(1 - x)$, which for $x = 0.5$ gives $\langle r \rangle = 2.0$ or $N_{SiO_{nb}} = 2.0$, and this is clearly larger than the value $N_{SiOnb} = 1.55$ observed in the current study. For hydroxyls, the contribution to eq 4 is $(2 - 2x + y)/(1 - x)$, which for $x = 0.5$ gives $\langle r \rangle = 3.2$ or $N_{SiO_h} = 0.8$. Again, this is clearly larger than the observed value of $N_{SiO_h} = 0.4$. This implies that there are some O_{nb} and/or O_h that are not coordinated to Si (and hence are not reducing network connectivity).

The presence of oxygens that are not coordinated to Si can be determined by inspecting the models. It is found that, for all x, all O_{nb} are coordinated to 1 Si. In addition, for $x = 0$, all O_h are coordinated to 1 Si. However, for $x > 0$, some O_h are coordinated to 1 Si, and some are coordinated to 0 Si. For $x = 0.5$, the observed value of $N_{SiO_h} = 0.4$ is only 50% of the predicted value of $N_{SiO_h} = 0.8$ because 50% of the hydroxyls are not coordinated to Si. The segregated O_h must be coordinated to Ca (the only other positive ion), which reduces the effect of Ca in breaking Si−O−Si connections. That is, the observed value of $N_{SiO_{nb}} = 1.55$ is consistent with the predicted value of $N_{SiO_{nb}} = 2.0$ reduced by the amount 0.4 because of the 50% of hydroxyls that are segregated. The tendency for isolated hydroxyls to coordinate to Ca can be connected to the basic and acidic natures of CaO and SiO_2, respectively.[36]

4.3. Effect of Hydroxyls on Ca Coordination. The coordination of Ca in the current study differs in three respects from that observed in recent models of $CaSiO_3$ melt-quenched glass.[11] First, although the main contribution to Ca−O coordination is from O_{nb}, it is ∼30% lower than that in melt-quenched glasses. For x from 0.1 to 0.5, the current study has $N_{CaO_{nb}}$ values from 2.4 to 3.7, whereas for melt-quenched glass models, the value was $N_{CaO_{nb}} = 5.4$ at $x = 0.5$. This can be explained as consequence of segregation of O_h (i.e., O_h, which is coordinated to Ca and not Si), which reduces the amount of O_{nb} present, as discussed in Section 4.2. Because all O_{nb} is coordinated to Si, the reduction in O_{nb} is demonstrated by the value of $N_{SiO_{nb}} = 1.55$ in the current study being ∼20% lower than $N_{SiO_{nb}} = 2.0$ found in melt-quenched glass model, which is fairly consistent with $N_{CaO_{nb}}$ in the current study being ∼30% lower than $N_{CaO_{nb}} = 5.4$ found in the melt-quenched glass model.

Second, the contribution to Ca−O coordination from O_b is minor, with a value of $N_{CaO_b} \approx 0.6$ for all x in the current study. Although the value of $N_{CaO_b} \approx 0.6$ is minor, it nevertheless represents a noteworthy feature of atomic structure. Using the relationship $x_i N_{ij} = x_j N_{ji}$ (where x_i is concentration) with $x = 0.5$ and $x_{O_{nb}} = x_{Si} N_{SiO_{nb}} = 0.8$ gives $N_{O_bCa} \approx 0.3$. Hence on average, 30% of O_b is bonded to 2 Si plus 1 Ca. These O_b can be expected to have weaker/longer Si−O_b bonds; in compensation, there will be some O_{nb} with stronger/shorter Si−O_{nb} bonds. There is evidence of this in the $T_{SiO}(r)$ (see Figure 1), which shows shorter Si−O_{nb} bonds. The sol−gel-derived models with $N_{CaO_b} \approx 0.6$ for all x are in contrast to the melt-quenched glass model, where $N_{CaO_b} = 1.0$ for $x = 0.5$. In melt-quenched glass models, O_b is the only alternative to O_{nb} for coordinating Ca. In sol−gel-derived models, O_b is less important, because O_h is available for coordinating to Ca.

Third, in sol−gel-derived models, the O_h provides coordination to Ca. A substantial contribution of $N_{CaO_h} \approx 1.6$ is observed in the current study. This is approximately constant in x, but it is important to distinguish two cases. At low x, most hydroxyls are coordinated to Si, i.e., Si−O_h−H configurations. These are similar to Si−O_b−Si configurations in that both contain an oxygen with two single bonds, and hence at low x, the O_h can be expected to replace O_b in coordinating Ca. Note that Ca coordination to O_h in Si−O_h−H configurations is preferable to O_b in Si−O_b−Si configurations because there is less repulsion between cations. As x increases, there is a decrease in Si−O_h−H configurations, but an increase in segregated hydroxyls. The latter are similar to Si−O_{nb} configurations in that both contain a singly bonded oxygen, and hence at high x, the O_h can be expected to play a similar role to O_{nb} in coordinating Ca. Thus it seems understandable that O_h makes a substantial contribution to Ca−O coordination for both low and high x.

4.4. The distribution of Ca. It is important to examine the distribution of Ca in these materials, because dissolution

(35) Chiari, G. *Acta Crystallogr., Sect. B* **1990**, *46*, 717.

(36) Gill, R. *Chemical Fundamentals of Geology*; Chapman and Hall: London, 1996; p 175.

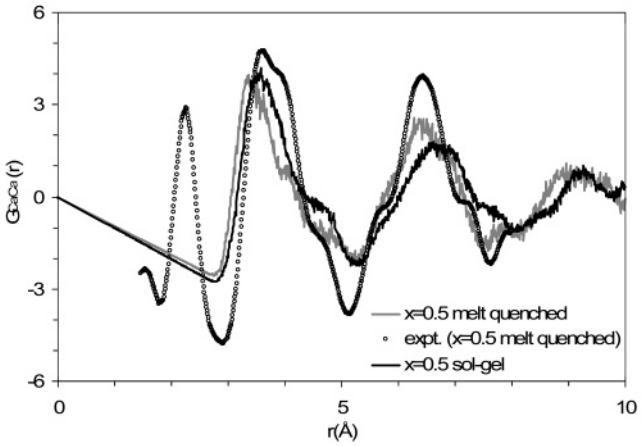

Figure 10. Ca−Ca distribution function, $G_{CaCa}(r) = T_{CaCa}(r) - 4\pi r\rho_{Ca}$, for $x = 0.5$ from (black line) sol−gel derived and (grey line) melt-quenched glass models, and (points) from melt-quenched glass experimental double-difference neutron diffraction with isotopic substitution[37] (in the original study,[37] the peak at ∼2.4 Å is attributed to an artifact arising from incomplete subtraction of Ca−O correlations).

of Ca is a crucial step in bioactivity. One measure of the distribution of Ca is the average number of Ca−Ca neighbors, N_{CaCa}, defined using a cutoff of 5.0 Å corresponding to the minimum in $T_{CaCa}(r)$. For $(CaO)_x(SiO_2)_{1-x}$ melt-quenched glass models, the average value is $N_{CaCa} = 7.0$ for $x = 0.5$. The results for sol−gel-derived models are shown in Table 4. The average value of $N_{CaCa} = 6.7$ for $x = 0.5$ is similar to that expected for a homogeneous distribution, in which many Ca−Ca neighbors will occur by chance. (In a random distribution with $x = 0.5$, a sphere of radius 5.0 Å would contain on average 6.7 Ca). It is less than the maximal values of $N_{CaCa} = 8$ for portlandite $Ca(OH)_2$ and $N_{CaCa} = 12$ for lime CaO. The average value of $N_{CaCa} = 1.9$ for $x = 0.1$ is greater than expected for a homogeneous distribution. (In a random distribution with $x = 0.1$, a sphere of radius 5.0 Å would contain on average 1.0 Ca). The value of $N_{CaCa} = 1.8$ suggests a distribution of Ca in clusters of 2 or 3 and is consistent with the value of $N_{O_{nb}Ca} = 1.3$ (calculated from $N_{CaO_{nb}} = 2.38$ for $x = 0.1$, using $x_i N_{ij} = x_j N_{ji}$), i.e., on average, 30% of O_{nb} are shared by 2 Ca.

Another description of the Ca distribution is given by $T_{CaCa}(r)$. Figure 10 shows the closely related function $G_{CaCa}(r) = T_{CaCa}(r) - 4\pi r\rho_{Ca}$. The Ca−Ca correlation for the $x = 0.5$ sol−gel-derived model is similar to that for $x = 0.5$ melt-quenched glass, both model[11] and experimental[37] values (in the original study,[37] the peak at ∼2.4 Å is attributed to an artifact arising from incomplete subtraction of Ca−O correlations). The main difference is that the sol−gel-derived model has peaks in $G_{CaCa}(r)$ at slightly larger distances, which can be attributed to a lower density equal to 90% of melt-quenched glass density. Figure 11 shows an image of the $x = 0.3$ sol−gel-derived model, and there is no recognizable structure in the Ca distribution. In particular, there is no arrangement of Ca in sheets, which was previously proposed as a description of Ca ordering in calcium silicate glass.[37] The nature of connections between neighboring CaO_N polyhedra was investigated by calculating the numbers of oxygen that are shared by a given pair of connected CaO_N polyhedra (this analysis excluded some "isolated" CaO_N polyhedra that are present without having connected, neighboring CaO_N polyhedra). Average values of ∼1.5 were obtained for all x, indicating a roughly equal mixture of corner- and edge-sharing by neighboring CaO_N polyhedra. This was also found in melt-quenched glass models and is less than the 100% edge-sharing found in crystalline $CaSiO_3$ wollastonite.

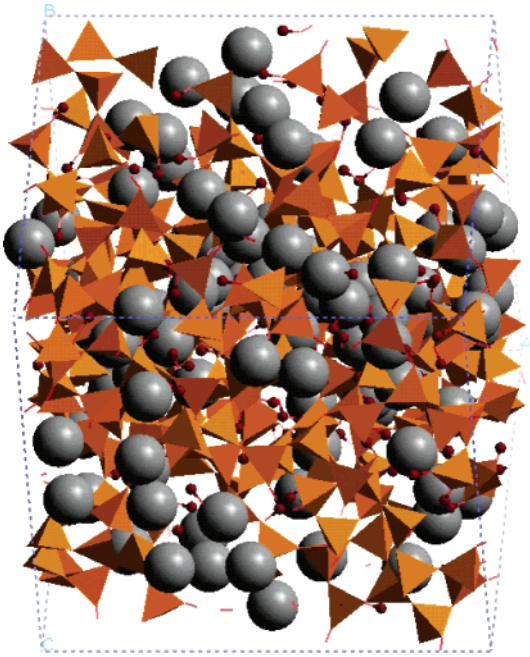

Figure 11. Image of $x = 0.3$ model, showing SiO_4 tetrahedra, Ca (large spheres), and H (small spheres).

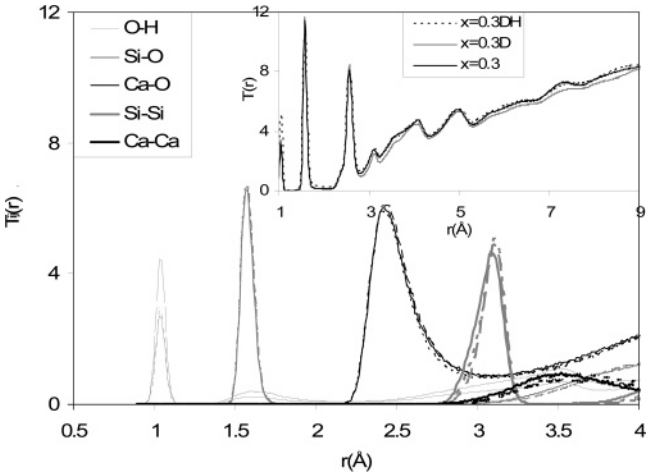

Figure 12. Radial distribution functions, $T_{ij}(r)$, for models (solid lines) $x = 0.3$, (dotted lines) $x = 0.3$ D, and (dashed lines) $x = 0.3$ DH (Si−O correlations have been scaled ×1/4). The inset shows $T(r)$. (Note that O refers to all types of oxygen.)

4.5. Effect of Density and Hydroxyl Content. Additional models were obtained to investigate the sensitivity of local atomic structure to density and hydroxyl content (y), because these are key parameters. Tables 3 and 4 include coordination numbers for the models with lower density, denoted $x = 0.3$ D, and for the models with greater hydroxyl content, denoted $x = 0.3$ DH, and Figure 12 shows selected $T_{ij}(r)$

(37) Gaskell, P. H.; Eckersley, M. C.; Barnes, A. C.; Chieux, P. *Nature* **1991**, *350*, 675.
(38) Skipper L. J. 2004, private communication.

and the inset shows total pair distribution functions $T(r)$. Whereas a change in density alters the slope of $T(r)$ at large values of r, the changes in short-range-order peaks $T(r)$ in the region 1−5 Å are smaller than those produced by changes in Ca content (see Figure 6). Comparing the models $x = 0.3$ and $x = 0.3$D, it is observed that the coordination of Si does not change, whereas for Ca, there is no change in $N_{CaO_{nb}}$ but a decrease in N_{CaO_b} and N_{CaO_h}. This is understandable if the stronger parts of the atomic structure are the Si−O_b−Si, Si−O_{nb}−Ca, and Si−O_h−H configurations, and these remain intact when the atomic volume is increased by reducing density. It appears that the weaker parts are Ca coordinated to O_b in Si−O_b−Si configurations and to O_h in Si−O_h−H configurations, and these are fractured. Comparing the models $x = 0.3$ (with $y = 0.2$) and $x = 0.3$ DH (with $y = 0.3$), it is observed that Si and Ca increase their coordination to O_h by 50%, as expected for an increase from $y = 0.2$ to $y = 0.3$. For Si, this has the effect of further reducing the silica network connectivity. For Ca, the increase in N_{CaO_h} is approximately balanced by a decrease in $N_{CaO_{nb}}$ (due to segregation of O_h). Increasing y seems to cause N_{CaCa} to decrease by 20%, suggesting that the Ca distribution is more homogeneous (on the scale of spherical regions of radius 5 Å, as discussed above), which may be associated with greater reduction of the silica network connectivity.

Conclusions

The molecular dynamics method used in the current study has been successful in producing for the first time detailed models of the local atomic structures of sol−gel-derived calcium silicates. These models specifically incorporate the features of being under-dense and hydrated, with H present as hydroxyl groups. The models are in satisfactory agreement with recent experimental results and show a tetrahedral silica network, with reduced network connectivity due to Ca and hydroxyls. Ca coordination is ∼6 for $x = 0.5$ and decreases as x decreases, and Ca is coordinated mostly to nonbridging oxygens, but with a small contribution from bridging oxygens (all features that are similar to those of melt-quenched glasses). Hydroxyls have a dramatic impact on the local atomic structure of the sol−gel-derived materials. Hydroxyls bonded to Si form Si−O−H configurations, but there is also coordination of isolated hydroxyls to Ca, which reduces the amount of nonbridging oxygen bonded to Si (and hence increases connectivity of the silica network). There is a substantial contribution to Ca coordination from hydroxyl groups. The Ca distribution for $x = 0.5$ is similar to that seen in $CaSiO_3$ melt-quenched glasses. For $x \rightarrow 0.1$, there is some clustering of Ca greater than that expected for a random distribution. The role of hydroxyls in coordinating to Ca is expected to enhance the dissolution of Ca and hence the bioactivity in comparison to that in melt-quenched glasses.

Acknowledgment. We are grateful for funding from EPSRC, U.K. We thank R.J. Newport and colleagues for access to experimental data prior to publication and an anonymous reviewer for helpful criticisms.

CM0527975